

**Validation of OSIRIS
mesospheric
temperatures**

P. E. Sheese et al.

This discussion paper is/has been under review for the journal Atmospheric Measurement Techniques (AMT). Please refer to the corresponding final paper in AMT if available.

Validation of OSIRIS mesospheric temperatures using satellite and ground-based measurements

**P. E. Sheese¹, K. Strong¹, E. J. Llewellyn², R. L. Gattinger², J. M. Russell III³,
C. D. Boone⁴, M. E. Hervig⁵, R. J. Sica⁶, and J. Bandoro⁶**

¹Department of Physics, University of Toronto, Toronto, Ontario, Canada

²ISAS, Department of Physics and Engineering Physics, University of Saskatchewan, Saskatoon, Saskatchewan, Canada

³Center for Atmospheric Sciences, Hampton University, Hampton, Virginia, USA

⁴Department of Chemistry, University of Waterloo, Waterloo, Ontario, Canada

⁵GATS Inc., Driggs, Idaho, USA

⁶Department of Physics and Astronomy, University of Western Ontario, London, Ontario, Canada

Received: 10 July 2012 – Accepted: 26 July 2012 – Published: 13 August 2012

Correspondence to: P. E. Sheese (psheese@atmosph.physics.utoronto.ca)

Published by Copernicus Publications on behalf of the European Geosciences Union.

Title Page

Abstract

Introduction

Conclusions

References

Tables

Figures

◀

▶

◀

▶

Back

Close

Full Screen / Esc

Printer-friendly Version

Interactive Discussion



Abstract

The Optical Spectrograph and InfraRed Imaging System (OSIRIS) on the Odin satellite is currently in its 12th year of observing the Earth's limb. For the first time, continuous temperature profiles extending from the stratopause to the upper mesosphere have been derived from OSIRIS observations of Rayleigh-scattered sunlight. OSIRIS temperatures are in good agreement with coincident temperature profiles derived from other satellite and ground-based measurements. In the altitude region of 55–80 km, OSIRIS temperatures are typically within 4–5 K of those from the SABER, ACE-FTS, and SOFIE instruments on the TIMED, SciSat-I, and AIM satellites, respectively. OSIRIS temperatures are typically within 2 K of those from the University of Western Ontario's Purple Crow Lidar in the altitude region of 50–79 km.

1 Introduction

Unlike in the lower atmosphere, where increases in CO₂ ultimately give rise to a heating effect, in the middle atmosphere, due to CO₂ relaxation through spontaneous emission into space, an increase in CO₂ ultimately leads to a cooling effect (e.g. Berger and Dameris, 1993; Schmidt et al., 2006). It is essential that there be continuous long-term measurements of middle atmospheric temperatures so as to determine the natural variability and to assess the consequences of natural and anthropogenic changes in CO₂ concentrations in this region. A new research product of mesospheric temperatures has been derived from Rayleigh-scattered sunlight observations from the Optical Spectrograph and InfraRed Imaging System (OSIRIS) on the Odin satellite. In order to assess the validity of the OSIRIS mesospheric temperatures, the new OSIRIS research product is compared with coincident temperature profiles from the satellite-based instruments Sounding of the Atmosphere using Broadband Emission Radiometry (SABER), Atmospheric Chemistry Experiment – Fourier Transform Spectrometer

AMTD

5, 5493–5526, 2012

Validation of OSIRIS mesospheric temperatures

P. E. Sheese et al.

Title Page

Abstract

Introduction

Conclusions

References

Tables

Figures

⏪

⏩

◀

▶

Back

Close

Full Screen / Esc

Printer-friendly Version

Interactive Discussion



(ACE-FTS), and Solar Occultation For Ice Experiment (SOFIE), as well as the ground-based Purple Crow Lidar (PCL), located near London, Ontario, Canada.

The Odin satellite was launched into a sun-synchronous orbit in February 2001, and the OSIRIS instrument has been observing the Earth's limb ever since. Primarily designed to derive concentrations of ozone and ozone-related species in the stratosphere, OSIRIS has been providing high-quality information on the state of the atmosphere from the upper troposphere to the lower thermosphere throughout its extensive mission. As Odin nods in orbit, the OSIRIS instrument scans the Earth's limb between ~ 7 and 110 km, with a near 1-km vertical resolution and ~ 0.5 km pointing accuracy. Due to its polar orbit, OSIRIS observes between latitudes of 82° N and 82° S, however, daytime conditions are observed mainly in the summer hemisphere. The nominal Odin ascending/descending node is 06:00/18:00 LT, however the Odin orbit drifted towards later local times to ~ 06:40/18:40 LT in 2009. Currently, Odin's orbit is drifting back towards earlier local times. The OSIRIS optical spectrograph (OS) observes scattered sunlight and airglow emission in the near UV to near IR from 275–810 nm, with a near 1-nm spectral resolution. Within this spectral range there is, among many other features, broadband O₃ absorption in the Hartley bands at wavelengths less than ~ 320 nm, broadband NO₂ absorption between roughly 300–600 nm, and O₂ A-band absorption and/or emission near 762 nm. How these features are related to the OSIRIS temperature retrievals is discussed in the following section.

The SABER instrument on the Thermosphere-Ionosphere-Mesosphere Energetics and Dynamics (TIMED) satellite (Russell et al., 1999) was launched into orbit in December 2001. SABER observes the Earth's limb perpendicular to its orbital plane, scanning the limb from the surface to the thermosphere with a roughly 2-km vertical resolution. The nominal latitudinal coverage in north-viewing mode is between 83° N and 52° S and in south-viewing between 83° S and 52° N. Unlike Odin, TIMED is not in a sun-synchronous orbit, and it takes approximately 60 days for SABER to cover 24 h of local time. The SABER version 1.07 (v1.07) daytime temperatures (Remsberg et al.,

**Validation of OSIRIS
mesospheric
temperatures**

P. E. Sheese et al.

Title Page

Abstract

Introduction

Conclusions

References

Tables

Figures



Back

Close

Full Screen / Esc

Printer-friendly Version

Interactive Discussion



2008), used in this study, are derived from radiance measurements in the CO₂ 15- μ m rotation-vibration band.

The ACE-FTS instrument on the Canadian SciSat-I satellite (Bernath et al., 2005) was launched into a circular orbit in August 2003. ACE-FTS is a solar occultation instrument and derives two temperature profiles per orbit with an approximately 4-km vertical resolution. Temperature profiles are retrieved between \sim 12 and 115 km from observations of CO₂ absorption in a range of microwindows, mostly near the 4.3- μ m band (Boone et al., 2005). Both version 2.2 (v2.2) and version 3.0 (v3.0) of the level 2 ACE-FTS temperatures employ sets of microwindows near 940 cm⁻¹, 1890–1975 cm⁻¹, 2040–2075 cm⁻¹, 2275–2395 cm⁻¹, and 2405–2450 cm⁻¹; and v2.2 employed a set of microwindows in the range 3300–3380 cm⁻¹. Both v2.2 and v3.0 temperatures are compared with OSIRIS in this study.

The SOFIE instrument on the Aeronomy of Ice in the Mesosphere (AIM) satellite also observes Earth's limb using solar occultation. AIM was launched in April 2007 into a 12:00 a.m./p.m. sun-synchronous orbit, and SOFIE retrieves temperature profiles between 15 and 95 km, with a \sim 1.5-km vertical resolution, and between latitudes of approximately 65° and 85° in both the northern and southern hemispheres (Russell et al., 2009). The SOFIE temperatures are retrieved from broadband CO₂ absorption observations in the 4.3- μ m band (Marshall et al., 2011).

The Purple Crow Lidar (PCL) at the University of Western Ontario (42.9° N, 278.6° E) is capable of deriving temperature from measurements of Rayleigh-scattering in the altitude range of 30–100 km, and the details of the lidar system are given by Sica et al. (1995). The Rayleigh-scatter measurements are proportional to density, which assuming hydrostatic equilibrium and the Ideal Gas Law can be converted into temperature (e.g. Hauchecorne and Chanin, 1980). The temperature retrieval process for the PCL is discussed by Argall and Sica (2007) in the context of comparisons with existing temperature climatologies. Temperature profiles are retrieved between sunset and sunrise with an integration time of approximately one minute, and in order to increase signal-to-noise at the higher altitudes (greater than \sim 90 km) profiles within one-hour

Validation of OSIRIS mesospheric temperatures

P. E. Sheese et al.

Title Page

Abstract

Introduction

Conclusions

References

Tables

Figures

◀

▶

◀

▶

Back

Close

Full Screen / Esc

Printer-friendly Version

Interactive Discussion



intervals are co-added. For the one hour retrievals used in this study, the temperature integration process begins at a high enough altitude (greater than 95 km) such that by 80 km the uncertainty due to the chosen temperature at the top altitude level is insignificant.

5 The SABER v1.07 and ACE-FTS v2.2 temperature data have been rigorously validated. Remberg et al. (2008) reported that SABER v1.07 temperatures were on average lower than other satellite and ground-based temperature retrievals by ~ 1 K near the stratopause, and lower by ~ 2 K in the middle mesosphere. Sica et al. (2008) reported that ACE-FTS v2.2 temperatures typically agreed with other satellite and
10 ground-based temperature retrievals within 2 K in the stratosphere and within 5 K in the lower mesosphere, and in the mesosphere ACE-FTS temperatures exhibited a high bias of 3–6 K. Stevens et al. (2012) reported that SOFIE v1.2 temperatures below 85 km agree with SABER and ACE-FTS temperatures within ~ 4 K.

The following section describes the OSIRIS temperature retrievals in the mesosphere, Sect. 3 details and discusses temperature profile comparisons between OSIRIS and the abovementioned instruments, and a summary of the results is given in Sect. 4.

2 OSIRIS temperatures

At altitudes above ~ 60 km, OSIRIS observes O_2 A-band airglow emission near 762 nm. A-band limb-column emission spectrum profiles can be inverted to retrieve volume emission rate (VER) spectrum profiles. Temperatures can be derived from the VER profiles by fitting modelled temperature-dependent A-band spectra to the inverted spectra, as described by Sheese et al. (2010). The VER spectrum profiles are accurate enough for temperature retrievals at altitudes of ~ 85 km and above, where absorption
20 of the A-band airglow by O_2 is low. Below 85 km, A-band temperature retrievals are very susceptible to uncertainties in the O_2 density profile. As detailed by Sheese et
25

Validation of OSIRIS mesospheric temperatures

P. E. Sheese et al.

Title Page

Abstract

Introduction

Conclusions

References

Tables

Figures

◀

▶

◀

▶

Back

Close

Full Screen / Esc

Printer-friendly Version

Interactive Discussion



al. (2010, 2011), retrieved temperature accuracy is better than ± 6 K near 105 km, better than ± 3 K at 90 km, and better than ± 8 K at 85 km.

Below 85 km, temperatures are retrieved from observations of Rayleigh-scattered sunlight in the same manner that is often used with falling spheres and Rayleigh-scatter lidar systems (e.g. Bartman et al., 1956; Hauchecorne and Chanine, 1980), where temperature profiles are retrieved from the background density profile assuming hydrostatic equilibrium. The amount of Rayleigh-scattered sunlight OSIRIS observes is dependent on the background density profile.

Background density, $[M]$, profiles are retrieved from observations of Rayleigh-scattered sunlight in two different wavelength regions for retrievals in two different altitude regimes. For observations at tangent heights above 70 km, $[M]$ profiles are derived from mean observations near 318.5 nm (OS pixels 112–114); and for tangent heights at and below 70 km, $[M]$ profiles are derived from mean observations near 347.5 nm (OS pixels 186–188).

At high tangent heights, daytime OSIRIS observations are significantly contaminated by off-axis stray light, or baffle scatter. The majority of this stray light is due to solar radiation that has scattered off clouds or the Earth's surface below the satellite. Therefore, the baffle scatter signal is greatly reduced in spectral regions where there are large absorption bands, such as the O_3 Hartley bands below ~ 320 nm, and where there is less solar radiation. However, in this spectral region above ~ 80 km, OS observations can be near the detector noise threshold and therefore unreliable.

At 318.5 nm (OS pixels 112–114), the OS can detect Rayleigh-scattered sunlight, with insignificant baffle scatter contamination, up to tangent heights of ~ 85 –90 km. This wavelength region also avoids contamination from emission in the nearby OH ($A^2\Sigma \rightarrow X^2\Pi$) (1–1) band near 314 nm (Gattinger et al., 2008) and from the N_2 ($C^3\Pi_u \rightarrow B^3\Pi_g$) (1–0) band near 316 nm (Cleary et al., 1995). However, below ~ 55 km, O_3 absorption along the OSIRIS line-of-sight becomes significant at 318.5 nm. Therefore, in the lower altitude range of 45–72 km, $[M]$ profiles are retrieved from

**Validation of OSIRIS
mesospheric
temperatures**

P. E. Sheese et al.

Title Page

Abstract

Introduction

Conclusions

References

Tables

Figures

◀

▶

◀

▶

Back

Close

Full Screen / Esc

Printer-friendly Version

Interactive Discussion



**Validation of OSIRIS
mesospheric
temperatures**

P. E. Sheese et al.

Title Page

Abstract

Introduction

Conclusions

References

Tables

Figures

◀

▶

◀

▶

Back

Close

Full Screen / Esc

Printer-friendly Version

Interactive Discussion



observations near 347.5 nm. Below ~ 40 km, both O_3 and NO_2 absorption become significant near 347.5 nm. Retrievals at higher wavelengths, e.g. $\lambda > 650$ nm, where there is much less O_3 or NO_2 absorption are also not possible, since at these higher wavelengths there is significant contamination in the observed signal due to aerosol scattering. At this time, retrievals are simply limited to tangent height observations above 45 km, rather than incorporating simultaneous OSIRIS measurements of O_3 , NO_2 , or aerosol profiles into the retrieval. Scaled OS radiance profiles at 278, 318, and 347 nm for a single OSIRIS scan and a corresponding MSIS [M] profile (also scaled) are shown in Fig. 1a, and Fig. 1b shows the corresponding temperature retrieval along with temperature retrievals that only use density profiles derived from the individual spectral windows near 278, 318, and 347 nm.

In both wavelength regimes, [M] profiles are retrieved using the Newton iteration optimal estimation technique (Rodgers, 2008). Rayleigh-scattering cross-sections are calculated at each pixel wavelength according to the method detailed by Bucholtz (1995), and [M] profiles from the NRL-MSISE-00 model (Picone et al., 2003) corresponding to the OSIRIS observations are used as a priori profiles. In both wavelength regimes, the forward model assumes a constant solar flux, determined from the mean of 2003–2009 daily average spectral irradiance values from the Spectral Irradiance Monitor (SIM) instrument (Harder et al., 2005) on the Solar Radiation and Climate Experiment (SORCE) satellite (Sparn et al., 2005). SIM data was obtained from the SORCE website (http://lasp.colorado.edu/sorce/data/ssi_data.htm).

Retrievals at both 318.5 and 347.5 nm both assume only Rayleigh single scatter within the OSIRIS line-of-sight. Instead of incorporating a computationally expensive multiple-scatter model into the forward model, it was assumed that between 45 and 85 km, for each pixel the fraction of multiple-scatter to total signal is independent of height (Haley, 2008). Since the temperature retrievals are only sensitive to the density gradient, the density profiles retrieved near 347.5 nm were scaled to match those retrieved near 318.5 nm at the 70-km altitude level. As well, the only type of extinction

assumed in the forward model was Rayleigh scattering, according to the Beer-Lambert law.

Through the combination of the hydrostatic equation and the ideal gas law, it can be shown that,

$$T(z) = \frac{1}{n(z)} \left(n_0 T_0 - \frac{1}{k} \int_{z_0}^z g(z') n(z') m(z') dz' \right) \quad (1)$$

where $T(z)$ is the temperature at altitude z , n is the total number density, T_0 and n_0 are respectively the temperature and density at the initial altitude z_0 , k is Boltzmann's constant, g is the local gravitational acceleration, and m is the mean molecular mass of air. The local gravitational acceleration profile is approximated by,

$$g(z) = g_0 \left(\frac{R_E}{R_E + z} \right)^2 \quad (2)$$

where g_0 is the gravitational acceleration at the Earth's surface and R_E is the Earth's radius, assumed to be a perfect sphere. Temperatures are derived using Eqs. (1) and (2), using the retrieved [M] profiles spline-interpolated onto a 100-m grid and with T_0 equal to the A-band temperature at 85 km. The retrieved temperatures are then linearly interpolated onto a 1-km grid.

Uncertainties in the retrieved temperature profiles were determined by perturbing a given variable by its estimated uncertainty and comparing the perturbed temperature profile with the unperturbed profile. For each variable, the temperature uncertainty was the mean of differences between the perturbed and unperturbed retrievals of 100 profiles that were chosen randomly. The largest source of uncertainty in the temperature retrievals below 85 km is due to uncertainties in the temperature measurement at 85 km that is used as the top temperature estimate, T_0 , in the retrieval. As previously mentioned, the OSIRIS A-band temperatures have an estimated systematic uncertainty of 8 K at 85 km. A systematic uncertainty of 8 K in the top temperature estimate leads to

Validation of OSIRIS mesospheric temperatures

P. E. Sheese et al.

Title Page

Abstract

Introduction

Conclusions

References

Tables

Figures

◀

▶

◀

▶

Back

Close

Full Screen / Esc

Printer-friendly Version

Interactive Discussion



Validation of OSIRIS mesospheric temperatures

P. E. Sheese et al.

Title Page

Abstract

Introduction

Conclusions

References

Tables

Figures

◀

▶

◀

▶

Back

Close

Full Screen / Esc

Printer-friendly Version

Interactive Discussion



uncertainties at lower altitudes as given in Table 1. The next largest sources of uncertainty in the temperature retrievals, also shown in Table 1, are a systematic uncertainty of 10 % in the OSIRIS calibration and random errors due to instrument noise and a 2 % variation in solar flux at the top of the atmosphere. Temperature uncertainties due to deviations in the local gravitational acceleration and deviations of Earth's radius from that of a perfect sphere are less than 1 % at all retrieval altitudes. The total estimate of systematic uncertainties is less than 2 K at altitudes below 77 km and less than 1 K below 72 km.

One complication that arises is retrieving temperatures in the presence of a polar mesospheric cloud (PMC). PMCs are typically formed in the summer months at high latitudes near 82–87 km, and are readily detected by OSIRIS. Light scattered off a PMC will contaminate an OSIRIS profile at tangent heights at and below the altitude of the PMC, and thus will not contain solely Rayleigh-scattered radiation. Temperature retrievals are therefore limited to altitudes higher than 87 km for scans where a PMC is detected. Therefore any results shown for the summer polar regions will be reflective of that region in the absence of PMCs.

The OSIRIS temperature dataset has not yet been made publically available on the OSIRIS website, however can be made available through personal communication with the corresponding author.

3 Results

For each instrument dataset that is compared with OSIRIS, a separate subset of coincident OSIRIS data was created. All OSIRIS subsets and instrument datasets were filtered for outliers prior to comparing temperature profiles. Outliers for each individual dataset were determined using the Median Absolute Deviation (MAD) (e.g. Toohy et al., 2010; and references therein). Profiles were removed if at any altitude, the difference between the temperature and the median temperature at that altitude was greater than 3.5 times the MAD.

Validation of OSIRIS mesospheric temperatures

P. E. Sheese et al.

Title Page

Abstract

Introduction

Conclusions

References

Tables

Figures

◀

▶

◀

▶

Back

Close

Full Screen / Esc

Printer-friendly Version

Interactive Discussion



The 1σ standard deviation of temperature values for each dataset used in the following comparisons are shown in Fig. 2a. For each pair of datasets, the criteria for coincidence were that the individual observations had to be made within 1000 km and 1 h of each other. Figure 2a shows that in all four cases the OSIRIS temperature variations are on the same order as the dataset with which it is being compared. The only exception is in the PCL comparison, where OSIRIS variations increase significantly at altitudes above 82 km. This increase is due to one OSIRIS profile (out of 21 coincident profiles) that exhibits warmer temperatures than the others at these altitudes. However, the temperatures are not anomalously high considering the entire OSIRIS dataset, and therefore the profile has not been omitted. On average, the standard deviations increase with altitude from ~ 7 K to ~ 15 K and reflect the natural increase in temperature variability that occurs at higher altitudes and the variation exhibited in the measured OSIRIS A-band temperatures at 85 km. Since PCL measures temperature profiles throughout the night at a fixed location and can independently measure the statistical error, it is possible to make an estimate of the geophysical variability throughout a single night. The PCL temperature geophysical variability for each night when there was a coincident OSIRIS profile was calculated by taking the root mean square (RMS) variability throughout the night and subtracting the PCL statistical error, determined from the photon count statistics. As seen in Fig. 2b, the mean geophysical variability increases from approximately ± 2 K to ± 6 K throughout the altitude range.

The conditions for coincidence in the following comparisons were chosen separately for each instrument. The aim was to minimize both the spatial and temporal distances between coincident observations, while maintaining an appropriate number of coincident profiles for statistical relevance. In most cases, this trade-off leads to comparisons of measurements that are not true common-volume.

3.1 Comparisons with SABER

Since SABER is not in a sun-synchronous orbit, from 2002–2011 there were many opportunities for OSIRIS and SABER to make coincident observations, and due to

**Validation of OSIRIS
mesospheric
temperatures**

P. E. Sheese et al.

Title Page

Abstract

Introduction

Conclusions

References

Tables

Figures

◀

▶

◀

▶

Back

Close

Full Screen / Esc

Printer-friendly Version

Interactive Discussion



Odin's orbit the majority of the observations are in the AM. Figure 3 shows examples of coincident OSIRIS and SABER temperature retrievals that show good agreement in the overall vertical structure. There is a clear mesospheric inversion layer in both the OSIRIS and SABER retrieved profiles on 7 April 2004 near 80 km, Fig. 3a. As seen in Fig. 3b, on 23 July 2011, both the OSIRIS and SABER profiles exhibit a slight increase in temperature near 72 km and a stratopause extending from below 48 km to ~ 55 km.

Figure 4 shows the mean of differences between OSIRIS and SABER temperature profiles and the corresponding standard deviations for all coincident AM profiles between 2002 and 2011. For comparisons with coincident criteria of observations within a distance of 1000 km and observation time of 1 h, Fig. 4a, OSIRIS has a high bias of ~ 2 K in the lower to middle mesosphere, and near the stratopause OSIRIS has a low bias of 1–3 K. When comparing profiles that were observed within 100 km and 10 min, Fig. 4b, these biases remain roughly the same. With the stricter coincidence criteria, the low bias near the stratopause and the high bias in the lower to middle mesosphere are both on the order of 1–4 K.

The low bias near the stratopause appears to be latitude dependent, as seen in Figs. 5 and 6, which show how OSIRIS and SABER compare in different latitude regions near summer solstice and near equinox (September–October), respectively. At low latitudes, the low bias is on the order of 0–2 K, and at mid to high latitudes the low bias is on the order of 4–7 K. This could potentially be due to higher surface albedo at these latitudes, which leads to larger contribution from multiple-scattered solar radiation in the OSIRIS signal. Simulations show that not accounting for an increase in multiple-scatter in the observed signal leads to lower retrieved temperatures, whereas not accounting for an absorbing species would lead to higher retrieved temperatures.

At altitudes above 80 km, OSIRIS consistently exhibits a low bias of up to 15 K. As previously discussed, the top temperature estimate at 85 km has a significant influence on retrieved temperatures down to an altitude of approximately 70 km. The OSIRIS A-band temperatures (used for the top temperature estimate at 85 km) are known to be

lower than SABER values by ~ 12 K near the mesopause, and Sheese et al. (2011) outline possible reasons for this disagreement.

The standard deviation of the differences between coincident OSIRIS and SABER temperatures range from 2–6 K near 48 km and increases to 12–16 K near 84 km.

5 These standard deviations are within the variability of the individual datasets, shown in Fig. 2a.

3.2 Comparisons with ACE-FTS

As ACE-FTS is a solar occultation instrument and only scans the atmosphere twice per orbit, there are less coincident temperature data with which to compare. For this reason, the comparison results have only been separated into different latitude regions, and not into different seasons nor into local times. Before making any comparisons with the ACE-FTS data, all OSIRIS profiles were smoothed by the 4-km running mean in order to match the ACE-FTS vertical resolution. Comparisons are made between OSIRIS and both ACE-FTS v2.2 and v3.0 temperatures, although the v3.0 temperatures have yet to be officially validated. A few examples of OSIRIS – ACE-FTS comparisons that exhibit consistent large-scale vertical structure are shown in Fig. 7. Typically there is little difference between the ACE-FTS v2.2 and v3.0 temperatures, except in the case where the v2.2 profiles exhibit potentially unrealistic oscillations. As highlighted by Fig. 7c, the v3.0 retrievals are less susceptible to these oscillations, which typically results in temperature profiles that are more consistent with the OSIRIS data. However, some true vertical structure may be lost, as seen in Fig. 7c between 75 and 82 km.

Figure 8 shows the average differences between coincident OSIRIS and ACE-FTS temperature profiles and the corresponding standard deviations for both v2.2 and v3.0 temperatures from 2004–2011. The red dotted line in Figures 8a-d are at -4 K, indicating the previously reported 3–6 K high bias in the ACE-FTS v2.2 data (Sica et al., 2008). At all altitudes, OSIRIS temperatures have a low bias in comparison with those of ACE-FTS, and similar to the comparisons with SABER, OSIRIS temperatures exhibit

Validation of OSIRIS mesospheric temperatures

P. E. Sheese et al.

Title Page

Abstract

Introduction

Conclusions

References

Tables

Figures



Back

Close

Full Screen / Esc

Printer-friendly Version

Interactive Discussion



Validation of OSIRIS mesospheric temperatures

P. E. Sheese et al.

Title Page	
Abstract	Introduction
Conclusions	References
Tables	Figures
⏪	⏩
◀	▶
Back	Close
Full Screen / Esc	
Printer-friendly Version	
Interactive Discussion	



a much lower bias at the two altitude extremes. It can be seen that tightening the conditions for coincidence from distances less than 1000 km apart and observation times less than an hour apart, Fig. 8a and c, to 600 km and 30 min, Fig. 8b and d, does have a slight effect on the mean temperature difference when using the ACE-FTS v2.2 data.

5 However, above 55 km with the v3.0 data, the change in mean temperature difference due to tightening of the coincidence criteria is less than 0.5 K. Between 50 and 80 km, the low temperature bias seen with the v2.2 temperatures is improved by 0–2 K in the v3.0 comparisons, and above 80 km the bias is worsened by ~ 1 K. With the improved v3.0 temperatures, using the stricter coincidence criteria, OSIRIS and ACE-FTS temperatures agree within 4 K between ~ 55 and 80 km.

10 Comparisons between OSIRIS and ACE-FTS for different latitudinal regions are shown in Fig. 9. Again, the v3.0 data show an improvement of ~ 1 K at most heights and latitudinal regions. In the altitude region of 55–80 km, the OSIRIS and ACE-FTS v3.0 temperatures agree within 4 K in all latitudinal regions, with the exception of the northern mid-latitudes, where OSIRIS has a slightly lower temperature bias, near 5 K, at the lower altitudes.

15 The standard deviation of the temperature differences between coincident OSIRIS and ACE-FTS v2.2 and v3.0 temperatures range from 3–5 K near 48 km and increase to 7–11 K near 84 km. These standard deviations are within the variability of the individual datasets, shown in Fig. 2a.

3.3 Comparisons with SOFIE

25 The SOFIE dataset begins in May 2007, and all observations are poleward of 66° latitude, where OSIRIS is likely to detect a PMC and therefore not be able to retrieve a temperature profile. For these reasons, the comparisons between OSIRIS and SOFIE temperatures have only been separated into northern and southern hemispheric comparisons, with coincidence criteria of distances less than 1000 km apart and observation times less than an hour apart. Figure 10 shows examples of coincident OSIRIS and SOFIE temperature profiles that exhibit good agreement in large-scale vertical

structure. Multiple thermal inversions are seen in both the OSIRIS and SOFIE retrieved profiles on 11 September 2007, as seen in Fig. 10a. On 24 August 2008, OSIRIS and SOFIE retrieve temperatures in very good agreement above 60 km, below which both profiles exhibit a similar change in the temperature gradient, Fig. 10b.

Figure 11 shows the mean differences between coincident OSIRIS and SOFIE temperature profiles and corresponding standard deviations in the Arctic and Antarctic regions for 2007–2011. The Arctic data, Fig. 11a, are consistent with the ACE-FTS and the SABER comparisons, as well as with the findings of Stevens et al. (2012). In the Arctic, OSIRIS exhibits a low bias that ranges from 4 K near 55 km to 0 K near 70 km, and a high bias of ~ 2 K near 75 km. Again, OSIRIS exhibits a significant low bias below 55 km and above ~ 80 km. The mean difference is more negative in the Antarctic than in the Arctic; near 55 km OSIRIS exhibits a 7-K low bias, which improves to a ~ 2 -K low bias near 77 km. This larger low bias in the southern polar region than in the north was also a feature in the comparisons to summer SABER temperatures, Fig. 5e and j, indicating that OSIRIS retrievals may be more sensitive to uncertainties in the Antarctic region. This is most likely due to the higher surface albedo in the Antarctic, which leads to greater sensitivity to multiple scattering at higher altitudes.

The standard deviation of the differences between coincident OSIRIS and SOFIE Arctic temperatures increase from 5 K at 48 km and to 8 K at 84 km. In the Antarctic, standard deviations of the temperature differences decrease from 8 K at 48 km to 6 K near 65 km and then increase with altitude to 10 K at 84 km. These standard deviations are on the order of the variability of the individual datasets, shown in Fig. 2a.

3.4 Comparisons with PCL

Since PCL only retrieves temperature profiles for nighttime conditions and OSIRIS only retrieves temperatures during the day, there can never be truly coincident observations. However, since OSIRIS typically samples the mid-latitudes just after 06:00 a.m./p.m., it is possible to find retrieved profiles that are reasonably close in time. From the PCL dataset, between 2003 and 2007, 21 profiles were found to be measured within

Validation of OSIRIS mesospheric temperatures

P. E. Sheese et al.

Title Page

Abstract

Introduction

Conclusions

References

Tables

Figures



Back

Close

Full Screen / Esc

Printer-friendly Version

Interactive Discussion



1000 km and 5 h of an OSIRIS observation, 14 profiles within 1000 km and 2 h and 1000 km, and 8 profiles within an hour. With these criteria, the OSIRIS observations are made on average 101 min, 62 min, and 41 min later than PCL, respectively. It is not uncommon for these coincident profiles to show similar large-scale vertical structure, as seen in Fig. 12. On 8 August 2005, both OSIRIS and PCL measure a warming near 70 km, and on 23 May 2006, PCL measures an inversion layer near 80 km whereas OSIRIS measures a significant warming in the same region. Differences in the absolute temperatures are in part due to the compared profiles not being true common-volume, and, at the upper altitude levels, in part due to the OSIRIS low temperature bias at 85 km.

Figure 13 shows the mean differences between OSIRIS and PCL temperature profiles and the corresponding standard deviations for the three coincidence criteria listed above. There is very good agreement between OSIRIS and PCL in all three cases. OSIRIS temperatures are on average within ~ 2 K of the PCL values between 50 and 79 km. Again, OSIRIS exhibits a slight low bias at the lowest altitudes, and a much more significant low bias at the highest altitudes.

For all coincidence criteria, the standard deviation of the differences between coincident OSIRIS and PCL temperatures increase from ~ 4 K at 48 km to ~ 10 K near 80 km. These standard deviations are within the variability of the individual datasets, shown in Fig. 2a, however are greater than the PCL geophysical variability, shown in Fig. 2b. This is most likely due to the fact that the comparisons do not compare common volumes, but are separated in both time and geo-location. At the highest altitude levels, the standard deviations increase to ~ 15 K, this is due to the much larger variability in the OSIRIS data, which is reflective of the variation in measured A-band temperatures at 85 km.

Validation of OSIRIS mesospheric temperatures

P. E. Sheese et al.

[Title Page](#)[Abstract](#)[Introduction](#)[Conclusions](#)[References](#)[Tables](#)[Figures](#)[Back](#)[Close](#)[Full Screen / Esc](#)[Printer-friendly Version](#)[Interactive Discussion](#)

4 Summary

In the altitude range of 55–80 km, OSIRIS temperatures agree well with SABER and PCL temperature datasets, and are consistent with the ACE-FTS and SOFIE temperature biases discussed in previous studies. In this altitude range, the mean differences between coincident OSIRIS and SABER, ACE-FTS, and SOFIE temperatures are typically within 5 K. The exception is for observations in the Antarctic region at the lower end of this altitude range (near 55 km), where OSIRIS typically has a low bias on the order of 5–7 K. Below 55 km in all latitudinal regions and seasons, OSIRIS temperatures tend to exhibit a significant low bias. At these low altitudes and in the Antarctic region, the temperature retrievals require including a multiple-scatter radiative transfer model to determine the fraction of multiple-scatter to single-scatter ratio in the OSIRIS observations, as not accounting for multiple-scatter in the OSIRIS signal leads to lower retrieved temperatures at these low altitudes. Between altitudes of ~ 50 and 78 km, the mean difference between OSIRIS and PCL temperatures is typically within 2 K. Above ~ 80 km, OSIRIS temperatures are typically lower than those of all the other datasets, implying that there is a low bias in the initial A-band temperature used at the top retrieval altitude level of 85 km. Overall, in the 55–80 km range, OSIRIS is consistent with the other four datasets and is retrieving valid mesospheric temperature profiles.

Acknowledgements. This project was primarily funded by the Canadian Space Agency (CSA). Odin is a Swedish-led satellite project funded jointly by Sweden (Swedish National Space Board), Canada (CSA), France (Centre National d'Études Spatiales), and Finland (Tekes), with support by the 3rd party mission programme of the European Space Agency (ESA). The Atmospheric Chemistry Experiment is a Canadian-led mission mainly supported by the CSA. The Purple Crow Lidar would like to thank NSERC for its part in supporting this work.

AMTD

5, 5493–5526, 2012

Validation of OSIRIS mesospheric temperatures

P. E. Sheese et al.

Title Page

Abstract

Introduction

Conclusions

References

Tables

Figures

◀

▶

◀

▶

Back

Close

Full Screen / Esc

Printer-friendly Version

Interactive Discussion



References

- Argall, P. S. and Sica, R. J.: A comparison of Rayleigh and sodium lidar temperature climatologies, *Ann. Geophys.*, 25, 27-35, doi:10.5194/angeo-25-27-2007, 2007.
- Bartman, F. L., Chaney, L. W., Jones, L. M., and Liu, V. C.: Upper Air Density and Temperature by the Falling Sphere Method, *J. Appl. Phys.*, 27, 706–712, doi:10.1063/1.1722470, 1956.
- Berger, U. and Dameris, M.: Cooling of the upper atmosphere due to CO₂ increases: A model study, *Ann. Geophys.*, 11, 809–819, 1993, <http://www.ann-geophys.net/11/809/1993/>.
- Bernath, P. F., McElroy, C. T., Abrams, M. C., Boone, C. D., Butler, M., Camy-Peyret, C., Carleer, M., Clerbaux, C., Coheur, P.-F., Colin, R., DeCola, P., DeMazière, M., Drummond, J. R., Dufour, D., Evans, W. F. J., Fast, H., Fussen, D., Gilbert, K., Jennings, D. E., Llewellyn, E. J., Lowe, R. P., Mahieu, E., McConnell, J. C., McHugh, M., McLeod, S. D., Michaud, R., Midwinter, C., Nassar, R., Nichitiu, F., Nowlan, C., Rinsland, C. P., Rochon, Y. J., Rowlands, N., Semeniuk, K., Simon, P., Skelton, R., Sloan, J. J., Soucy, M.-A., Strong, K., Tremblay, P., Turnbull, D., Walker, K. A., Walkty, I., Wardle, D. A., Wehrle, V., Zander, R., and Zou, J.: Atmospheric Chemistry Experiment (ACE): Mission overview, *Geophys. Res. Lett.*, 32, L15S01, doi:10.1029/2005GL022386, 2005.
- Boone, C. D., Nassar, R., Walker, K. A., Rochon, Y., McLeod, S. D., Rinsland, C. P., and Bernath, P. F.: Retrievals for the Atmospheric Chemistry Experiment Fourier-Transform Spectrometer, *Appl. Optics*, 44, 7218–7231, doi:10.1364/AO.44.007218, 2005.
- Cleary, D. D., Gnanalingam, S., McCoy, R. P., Dymond, K. F., and Eparvier, F. G.: The Middle Ultraviolet Dayglow Spectrum, *J. Geophys. Res.*, 100, 9729–9739, doi:10.1029/94JA03145, 1995.
- Gattinger, R. L., Degenstein, D. A., Llewellyn, E. J., and Stevens, M. H.: OH $A^2\Sigma-X^2\Pi$ band ratios observed in the mesosphere by OSIRIS, *Can. J. Phys.*, 86, 857–862, doi:10.1139/P09-051, 2008.
- Haley, C. S.: Retrieval of Stratospheric Ozone and Nitrogen Dioxide Profiles From Odin Optical Spectrograph and Infrared Imager System (OSIRIS) Limb-Scattered Sunlight Measurements, Ph.D. Thesis, York University, Toronto, 2008.
- Harder, J. W., Fontenla, J., Lawrence, G., Woods, T., and Rottman, G.: The Spectral Irradiance Monitor: Measurement Equations and Calibration, *Solar Phys.*, 230, 169–204, doi:10.1007/s11207-005-1528-1, 2005.

Validation of OSIRIS mesospheric temperatures

P. E. Sheese et al.

Title Page

Abstract

Introduction

Conclusions

References

Tables

Figures

◀

▶

◀

▶

Back

Close

Full Screen / Esc

Printer-friendly Version

Interactive Discussion



Validation of OSIRIS mesospheric temperatures

P. E. Sheese et al.

Title Page

Abstract

Introduction

Conclusions

References

Tables

Figures

◀

▶

◀

▶

Back

Close

Full Screen / Esc

Printer-friendly Version

Interactive Discussion



- Hauchecorne, A. and Chanin, M.: Density and temperature profiles obtained by lidar between 35 and 70 km, *Geophys. Res. Lett.*, 7, 565–568, doi:10.1029/GL007i008p00565, 1980.
- Llewellyn, E. J., Lloyd, N. D., Degenstein, D. A., Gattinger, R. L., Petelina, S. V., Bourassa, A. E., Wiensz, J. T., Ivanov, E. V., McDade, I. C., Solheim, B. H., McConnell, J. C., Haley, C. S., von Savigny, C., Sioris, C. E., McLinden, C. A., Griffioen, E., Kaminski, J., Evans, W. F. J., Puckrin, E., Strong, K., Wehrle, V., Hum, R. H., Kendall, D. J. W., Matsushita, J., Murtagh, D. P., Brohede, S., Stegman, J., Witt, G., Barnes, G., Payne, W. F., Piché, L., Smith, K., Warshaw, G., Deslauniers, D. L., Marchand, E. H. Richardson, R.A. King, I. Wevers, W. McCreath, E. Kyrölä, L. Oikarinen, P., Leppelmeier, G. W., Auvinen, H., Mégie, G., Hauchecorne, A., Lefèvre, F., de La Noë, J., Ricaud, P., Frisk, U., Sjöberg, F., von Schéele, F., and Nordh, L.: The OSIRIS instrument on the Odin spacecraft, *Can. J. Phys.*, 82, 411–422, doi:10.1139/P04-005, 2004.
- Marshall, B. T., Deaver, L. E., Thompson, R. E., Gordley, L. L., McHugh, M. J., Hervig, M. E., and Russell III, J. M.: Retrieval of temperature and pressure using broadband solar occultation: SOFIE approach and results, *Atmos. Meas. Tech.*, 4, 893–907, doi:10.5194/amt-4-893-2011, 2011.
- Murtagh, D., Frisk, U., Merino, F., Ridal, M., Jonsson, A., Stegman, J., Witt, G., Eriksson, P., Jiménez, C., Megie, G., de la Noë, J., Ricaud, P., Baron, P., Pardo, J. R., Hauchecorne, Llewellyn, E. J., Degenstein, D. A., Gattinger, R. L., Lloyd, N. D., Evans, W. F. J., McDade, I. C., Haley, C. S., Sioris, C., von Savigny, C., Solheim, B. H., McConnell, J. C., Strong, K., Richardson, E. H., Leppelmeier, G. W., Kyrölä, E., Auvinen, H., and Oikarinen, L.: An overview of the Odin atmospheric mission, *Can. J. Phys.* 80, 309–319, doi:10.1139/P01-157, 2002.
- Picone, J. M., Hedin, A. E., Drob, D. P., and Aikin, A. C.: NRL-MSISE-00 empirical model of the atmosphere: Statistical comparisons and scientific issues, *J. Geophys. Res.*, 107, 1468, doi:10.1029/2002JA009430, 2002.
- Remsberg, E. E., Marshall, B. T., Garcia-Comas, M., Krueger, D., Lingenfelter, G. S., Martin-Torres, J., Mlynczak, M. G., Russell III, J. M., Smith, A. K., Zhao, Y., Brown, C., Gordley, L. L., Lopez-Gonzalez, M. J., Lopez-Puertas, M., She, C.-Y., Taylor, M. J., and Thompson, R. E.: Assessment of the quality of the Version 1.07 temperature-versus-pressure profiles of the middle atmosphere from TIMED/SABER, *J. Geophys. Res.*, 113, D17101, doi:10.1029/2008JD010013, 2008.
- Rodgers, C. D.: Inverse methods for atmospheric sounding, World Scientific Publishing Co., Singapore, 2008.

Validation of OSIRIS mesospheric temperatures

P. E. Sheese et al.

Title Page

Abstract

Introduction

Conclusions

References

Tables

Figures

◀

▶

◀

▶

Back

Close

Full Screen / Esc

Printer-friendly Version

Interactive Discussion



Russell III, J. M., Mlynczak, M. G., Gordley, L. L., Tansock, J., and Esplin, R.: An overview of the SABER experiment and preliminary calibration results, *P. Soc. Photo-Opt. Ins.*, 3756, 277–288, doi:10.1117/12.366382, 1999.

Russell III, J. M., Bailey, S. M., Gordley, L. L., Rusch, D. W., Horányi, M., Hervig, M. E., Thomas, G. E., Randall, C. E., Siskind, D. E., Stevens, M. H., Summers, M. E., Taylor, M. J., Englert, C. R., Espy, P. J., McClintock, W. E., and Merkel, A. W.: The Aeronomy of Ice in the Mesosphere (AIM) mission: Overview and early science results, *J. Atm. Sol.-Terr. Phys.*, 71, 289–299, doi:10.1016/j.jastp.2008.08.011, 2009.

Schmidt, H., Brasseur, G. P., Charron, M., Manzini, E., Giorgetta, M. A., and Diehl, T.: The HAMMONIA Chemistry Climate Model: Sensitivity of the Mesopause Region to the 11-Year Solar Cycle and CO₂ Doubling, *J. Climate*, 19, 3903–3931, doi:10.1175/JCLI3829.1, 2006.

Sheese, P. E., Llewellyn, E. J., Gattinger, R. L., Bourassa, A. E., Degenstein, D. A., Lloyd, N. D., and McDade, I. C.: Temperatures in the upper mesosphere and lower thermosphere from OSIRIS observations of O₂ A-band emission spectra, *Can. J. Phys.*, 88, 919–925, doi:10.1139/P10-093, 2010.

Sheese, P. E., Llewellyn, E. J., Gattinger, R. L., Bourassa, A. E., Degenstein, D. A., Lloyd, N. D., and McDade, I. C.: Mesopause temperatures during the polar mesospheric cloud season, *Geophys. Res. Lett.*, 38, L11803, doi:10.1029/2011GL047437, 2011.

Sica, R. J., Sargoytchev, S., Argall, P. S., Borra, E. F., Girard, L., Sparrow, C. T., and Flatt, S.: Lidar measurements taken with a large-aperture liquid mirror, 1. Rayleigh-scatter system, *Appl. Optics*, 34, 6925–6936, doi:10.1364/AO.34.006925, 1995.

Sica, R. J., Izawa, M. R. M., Walker, K. A., Boone, C., Petelina, S. V., Argall, P. S., Bernath, P., Burns, G. B., Catoire, V., Collins, R. L., Daffer, W. H., De Clercq, C., Fan, Z. Y., Firanski, B. J., French, W. J. R., Gerard, P., Gerding, M., Granville, J., Innis, J. L., Keckhut, P., Kerzenmacher, T., Klekociuk, A. R., Kyrö, E., Lambert, J. C., Llewellyn, E. J., Manney, G. L., McDermid, I. S., Mizutani, K., Murayama, Y., Piccolo, C., Raspollini, P., Ridolfi, M., Robert, C., Steinbrecht, W., Strawbridge, K. B., Strong, K., Stübi, R., and Thurairajah, B.: Validation of the Atmospheric Chemistry Experiment (ACE) version 2.2 temperature using ground-based and space-borne measurements, *Atmos. Chem. Phys.*, 8, 35–62, doi:10.5194/acp-8-35-2008, 2008.

Sparr, T. P., Rottman, G., Woods, T. N., Boyle, B. D., Kohnert, R., Ryan, S., Davis, R., Fulton, R., and Ochs, W.: The SORCE spacecraft and operations, *Solar Phys.*, 230, 71–89, doi:10.1007/s11207-005-1584-6, 2005.

Stevens, M. H., Deaver, L., Hervig, M. E., Rusell III, J. M., Siskind, D. E., Sheese, P. E., Llewellyn, E. J., Gattinger, R. L., Höffner, J., and Marshall, B. T.: Validation of Upper Mesospheric and Lower Thermospheric Temperatures Measured by the Solar Occultation For Ice Experiment, *J. Geophys. Res.*, doi:10.1029/2012JD017689, in press, 2012.

- 5 Toohy, M., Strong, K., Bernath, P. F., Boone, C. D., Walker, K. A., Jonsson, A. I., and Shepherd, T. G.: Validating the reported random errors of ACE-FTS measurements. *J. Geophys. Res.*, 115, D20304, doi:10.1029/2010JD014185, 2010.

AMTD

5, 5493–5526, 2012

Validation of OSIRIS mesospheric temperatures

P. E. Sheese et al.

Title Page

Abstract

Introduction

Conclusions

References

Tables

Figures

⏪

⏩

◀

▶

Back

Close

Full Screen / Esc

Printer-friendly Version

Interactive Discussion



Validation of OSIRIS mesospheric temperatures

P. E. Sheese et al.

Table 1. Uncertainties in retrieved OSIRIS temperatures. All uncertainty values are in Kelvin.

Altitude (km)	Top altitude temperature (T_o)	OSIRIS calibration	Total systematic	Instrument noise	Solar flux	Total random (one scan)
48	0.05	0.90	0.90	0.21	0.19	0.28
52	0.08	0.49	0.49	0.28	0.11	0.30
56	0.13	0.32	0.34	0.32	0.06	0.33
60	0.21	0.32	0.38	0.62	0.05	0.62
64	0.35	0.30	0.46	0.69	0.05	0.69
68	0.58	0.15	0.60	0.73	0.05	0.73
72	1.02	0.15	1.03	1.00	0.03	1.01
76	1.84	0.19	1.85	1.55	0.04	1.55
80	3.44	0.19	3.45	1.81	0.06	1.81
84	6.70	0.08	6.70	0.78	0.02	0.78

Title Page

Abstract

Introduction

Conclusions

References

Tables

Figures

◀

▶

◀

▶

Back

Close

Full Screen / Esc

Printer-friendly Version

Interactive Discussion



Validation of OSIRIS
mesospheric
temperatures

P. E. Sheese et al.

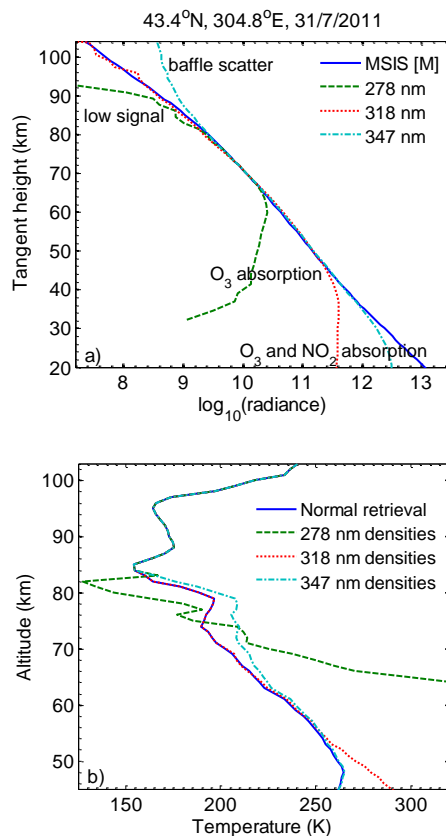


Fig. 1. (a) Comparison of scaled log OSIRIS limb radiance profiles at 278, 318, and 347 nm and the corresponding scaled MSIS background density profile. All profiles are scaled to match the 278 nm radiance value, in photons $\text{s}^{-1} \text{cm}^{-2} \text{sr}^{-1} \text{nm}^{-1}$, at 72 km. (b) Retrieved temperature profiles using the densities derived from the OSIRIS limb radiance profiles of (a).

Validation of OSIRIS mesospheric temperatures

P. E. Sheese et al.

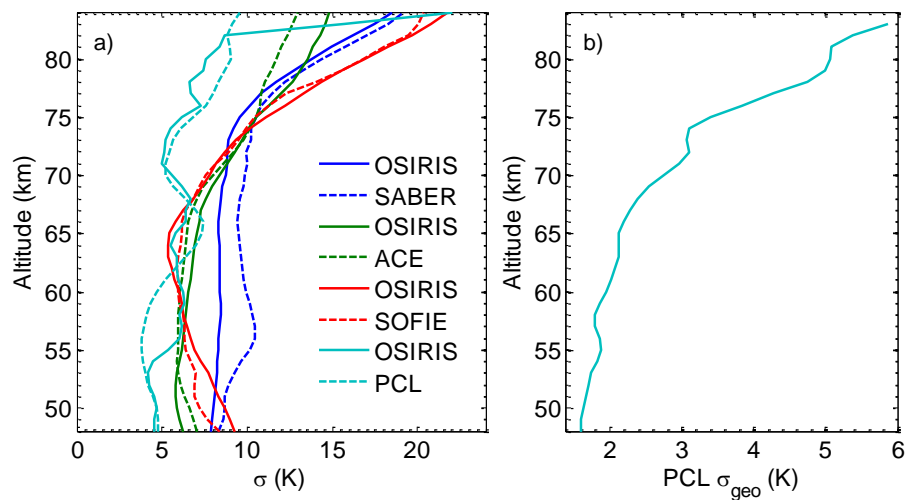


Fig. 2. (a) The 1 σ temperature variations of coincident datasets where the conditions for coincidence were observations made within 1000 km and within 1 h. (b) The mean PCL temperature geophysical variability for all nights when there was a coincident OSIRIS profile.

Title Page

Abstract

Introduction

Conclusions

References

Tables

Figures

◀

▶

◀

▶

Back

Close

Full Screen / Esc

Printer-friendly Version

Interactive Discussion



**Validation of OSIRIS
mesospheric
temperatures**

P. E. Sheese et al.

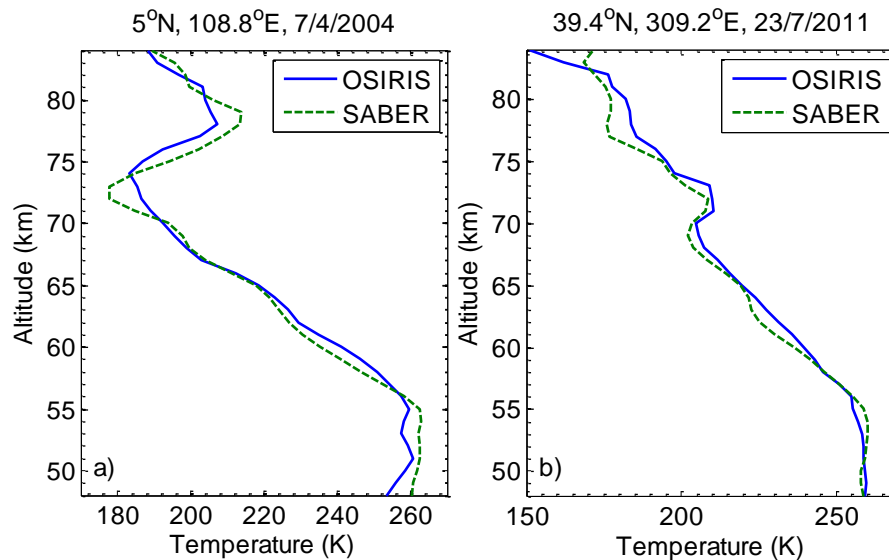


Fig. 3. Examples of coincident OSIRIS and SABER temperature profiles that exhibit agreement in large-scale vertical structure.

[Title Page](#)[Abstract](#)[Introduction](#)[Conclusions](#)[References](#)[Tables](#)[Figures](#)[◀](#)[▶](#)[◀](#)[▶](#)[Back](#)[Close](#)[Full Screen / Esc](#)[Printer-friendly Version](#)[Interactive Discussion](#)

**Validation of OSIRIS
mesospheric
temperatures**

P. E. Sheese et al.

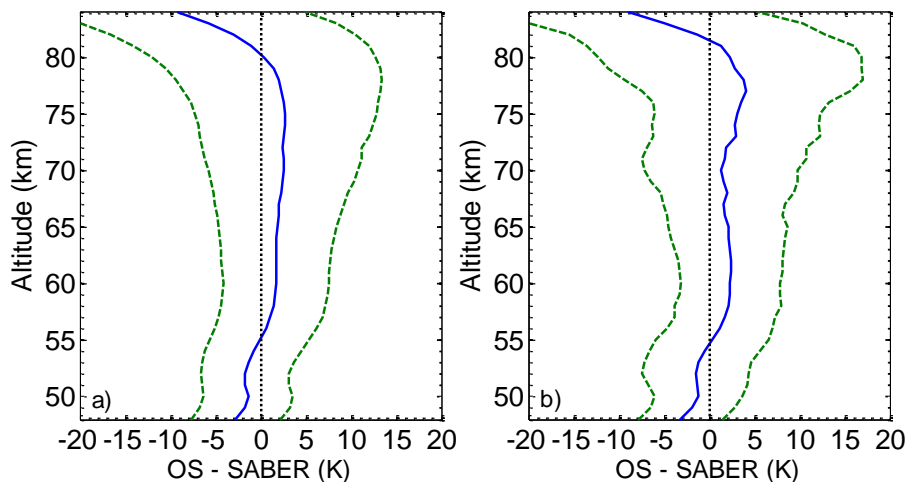


Fig. 4. Mean differences between OSIRIS and SABER AM temperatures (solid blue) and corresponding standard deviations (dashed green), for **(a)** 15 773 profiles measured within 1000 km and 1 h and **(b)** 143 profiles measured within 100 km and 10 min.

Title Page

Abstract

Introduction

Conclusions

References

Tables

Figures

◀

▶

◀

▶

Back

Close

Full Screen / Esc

Printer-friendly Version

Interactive Discussion



**Validation of OSIRIS
mesospheric
temperatures**

P. E. Sheese et al.

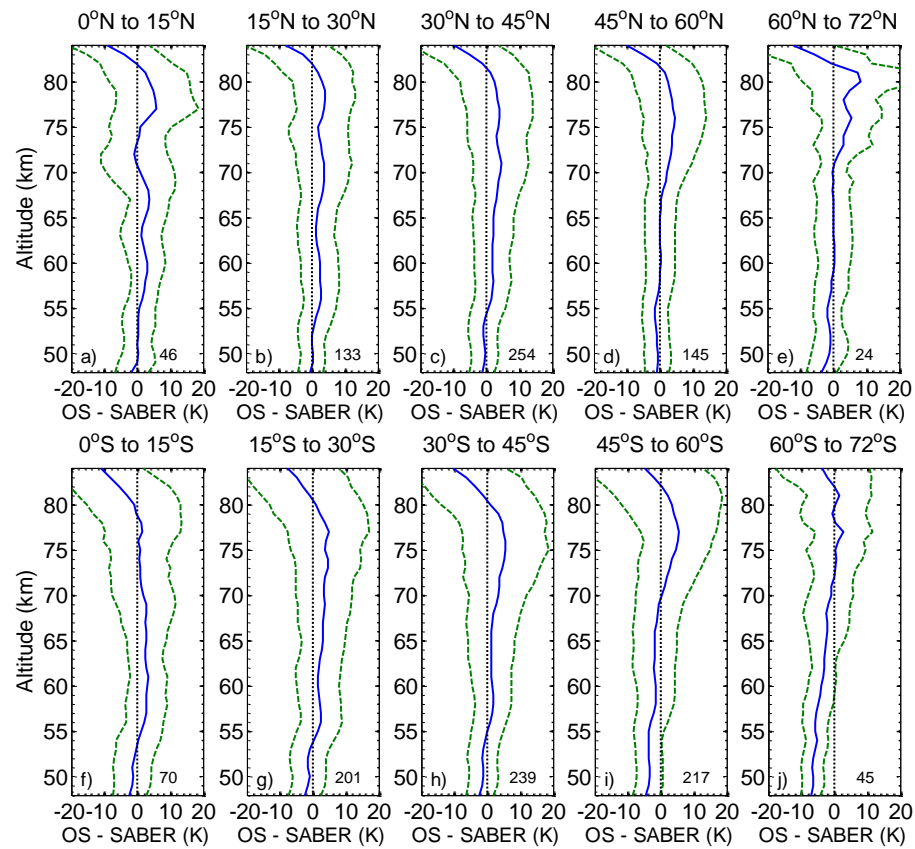


Fig. 5. Mean differences between OSIRIS and SABER AM temperatures (solid blue) and corresponding standard deviations (dashed green) for summer, AM profiles measured within 200 km and 1 h during June–July (top) and December–January (bottom). The number in the bottom right corner of each plot indicates the number of coincident profiles.

Title Page

Abstract Introduction

Conclusions References

Tables Figures

◀

▶

◀

▶

Back

Close

Full Screen / Esc

Printer-friendly Version

Interactive Discussion



**Validation of OSIRIS
mesospheric
temperatures**

P. E. Sheese et al.

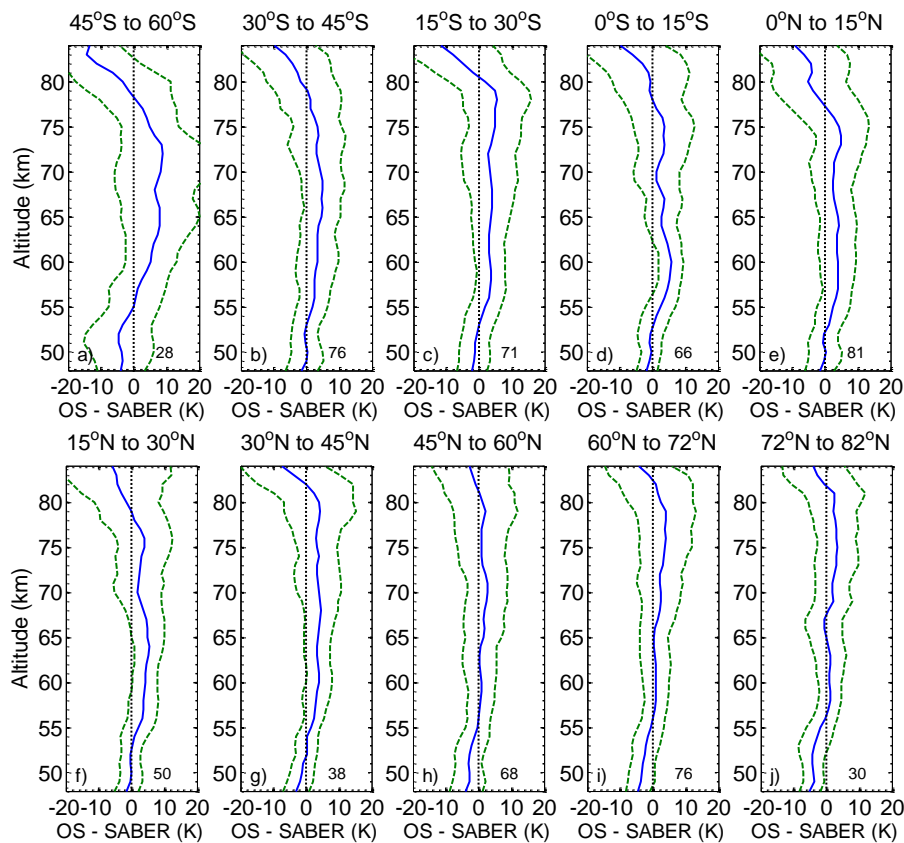


Fig. 6. Mean differences between OSIRIS and SABER AM temperatures (solid blue) and corresponding standard deviations (dashed green) for profiles measured within 200 km and 1 h during September–October. The number in the bottom right corner of each plot indicates the number of coincident profiles.

Title Page

Abstract Introduction

Conclusions References

Tables Figures

◀

▶

◀

▶

Back

Close

Full Screen / Esc

Printer-friendly Version

Interactive Discussion



**Validation of OSIRIS
mesospheric
temperatures**

P. E. Sheese et al.

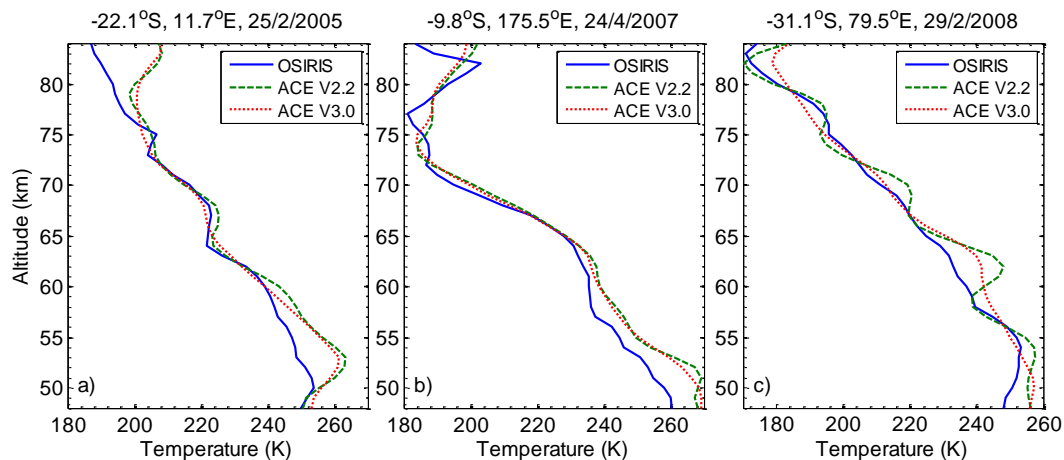


Fig. 7. Examples of coincident OSIRIS and ACE-FTS temperature profiles exhibiting similar large-scale vertical structure. OSIRIS profiles were smoothed by 4-km running mean in order to match the ACE-FTS vertical resolution.

Title Page

Abstract

Introduction

Conclusions

References

Tables

Figures

◀

▶

◀

▶

Back

Close

Full Screen / Esc

Printer-friendly Version

Interactive Discussion



**Validation of OSIRIS
mesospheric
temperatures**

P. E. Sheese et al.

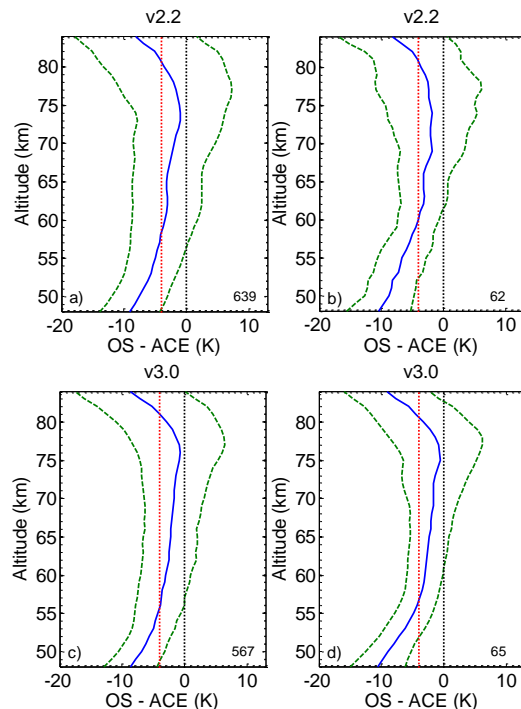


Fig. 8. Mean differences between OSIRIS and ACE-FTS temperatures (solid blue) and corresponding standard deviations (dashed green), for profiles measured within (left) 1000 km and 1 h, and (right) 600 km and 30 min. The top panel shows v2.2 data, the bottom panel shows v3.0, the red dotted line at -4 K indicates the known ACE-FTS v2.2 high temperature bias, and the number in the bottom right corner of each plot indicates the number of coincident profiles. OSIRIS profiles were smoothed by 4-km running mean in order to match the ACE-FTS vertical resolution.

Title Page

Abstract

Introduction

Conclusions

References

Tables

Figures

◀

▶

◀

▶

Back

Close

Full Screen / Esc

Printer-friendly Version

Interactive Discussion



Validation of OSIRIS mesospheric temperatures

P. E. Sheese et al.

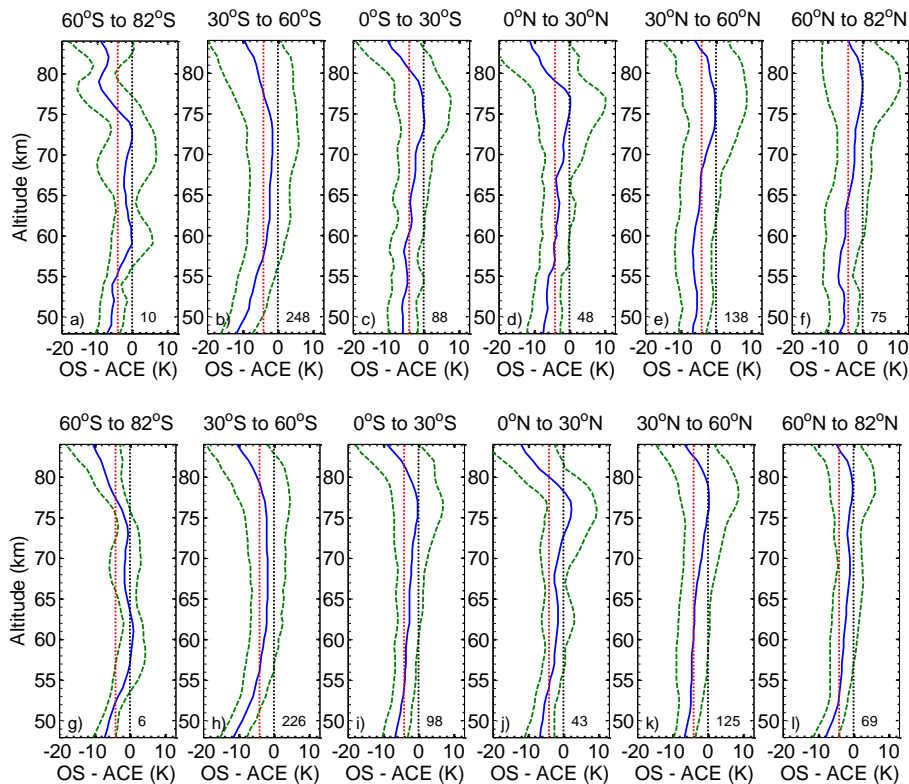


Fig. 9. Mean differences between OSIRIS and ACE-FTS temperatures (solid blue) and corresponding standard deviations (dashed green) for all profiles measured within 1000 km and 1 h. OSIRIS profiles were smoothed by 4-km running mean in order to match the ACE-FTS vertical resolution. The number in the bottom right corner of each plot indicates the number of coincident profiles, and the red dotted line at -4 K indicates the known ACE-FTS v2.2 high temperature bias. OSIRIS comparisons with **(a–f)** v2.2 data, **(g–l)** v3.0 data.

Title Page

Abstract Introduction

Conclusions References

Tables Figures

◀

▶

◀

▶

Back

Close

Full Screen / Esc

Printer-friendly Version

Interactive Discussion



Validation of OSIRIS mesospheric temperatures

P. E. Sheese et al.

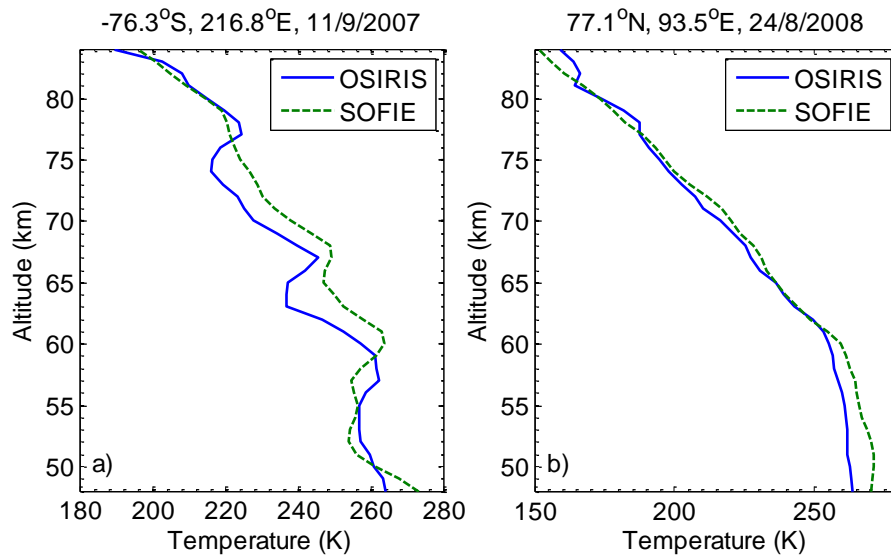


Fig. 10. Examples of coincident OSIRIS and SOFIE temperature profiles exhibiting similar large-scale vertical structure.

Title Page	
Abstract	Introduction
Conclusions	References
Tables	Figures
◀	▶
◀	▶
Back	Close
Full Screen / Esc	
Printer-friendly Version	
Interactive Discussion	



**Validation of OSIRIS
mesospheric
temperatures**

P. E. Sheese et al.

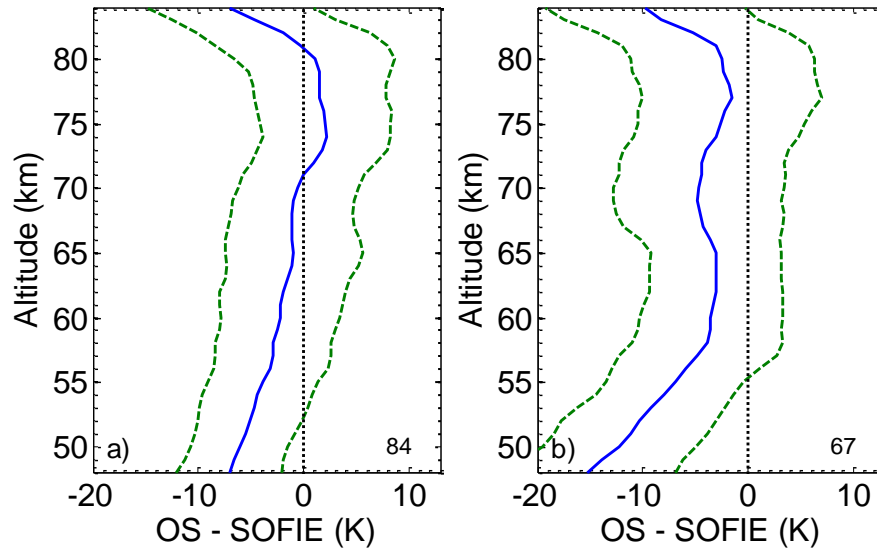


Fig. 11. Mean differences between OSIRIS and SOFIE temperatures (solid blue) and corresponding standard deviations (dashed green) for profiles measured within 1000 km and 1 h in the **(a)** Arctic and **(b)** Antarctic. The number in the bottom right corner of each plot indicates the number of coincident profiles.

Title Page

Abstract

Introduction

Conclusions

References

Tables

Figures

◀

▶

◀

▶

Back

Close

Full Screen / Esc

Printer-friendly Version

Interactive Discussion



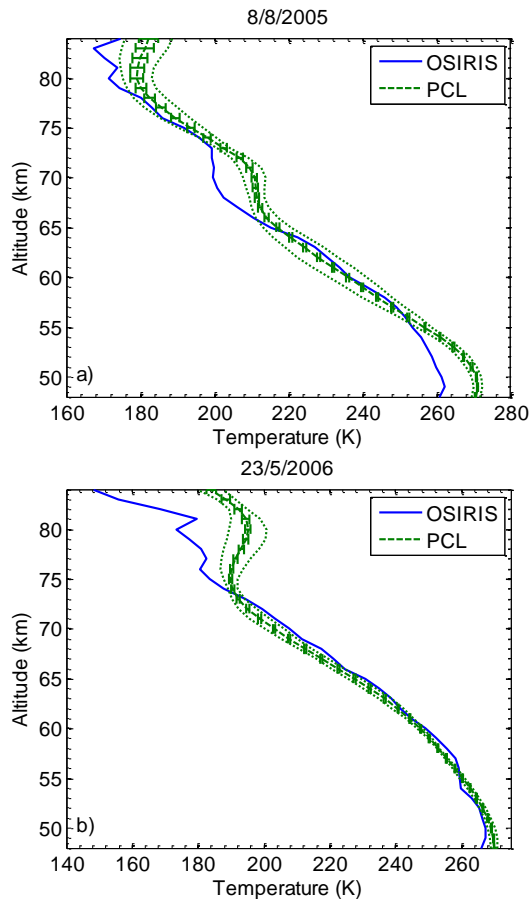


Fig. 12. Examples of coincident OSIRIS and PCL temperature profiles exhibiting similar large-scale vertical structure. The PCL error bars represent the statistical uncertainty and the green dotted lines represent the temperature geophysical variances (defined in text) on the night of observation.

Validation of OSIRIS mesospheric temperatures

P. E. Sheese et al.

Title Page

Abstract Introduction

Conclusions References

Tables Figures

◀ ▶

◀ ▶

Back Close

Full Screen / Esc

Printer-friendly Version

Interactive Discussion



**Validation of OSIRIS
mesospheric
temperatures**

P. E. Sheese et al.

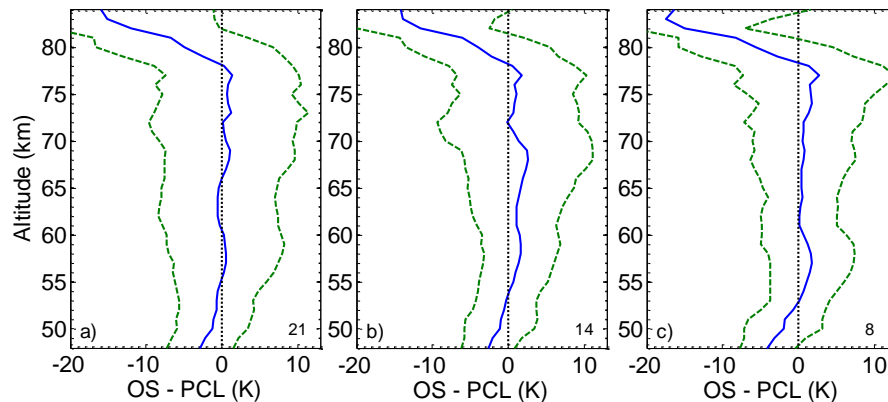


Fig. 13. Mean differences between OSIRIS and PCL temperatures (solid blue) and corresponding standard deviations (dashed green) for all profiles measured within 1000 km and **(a)** 5 h, **(b)** 2 h, and **(c)** 1 h. The number in the bottom right corner of each plot indicates the number of coincident profiles.

Title Page

Abstract

Introduction

Conclusions

References

Tables

Figures

◀

▶

◀

▶

Back

Close

Full Screen / Esc

Printer-friendly Version

Interactive Discussion

